Caramel Popcorn Shaped Silicon Particle with Carbon Coating as a High Performance Anode Material for Li-Ion Batteries

Meinan He,[†] Qina Sa,[†] Gao Liu,[‡] and Yan Wang*[,†]

[†]Mechanical Engineering, Worcester Polytechnic Institute, 100 Institute Road, Worcester, Massachusetts 01609, United States
[‡]Lawrence Berkeley National Laboratory, 1 Cyclotron Road, Berkeley, California 94720, United States

ABSTRACT: Silicon is a very promising anode material for lithium ion batteries. It has a 4200 mAh/g theoretical capacity, which is ten times higher than that of commercial graphite anodes. However, when lithium ions diffuse to Si anodes, the volume of Si will expand to almost 400% of its initial size and lead to the crack of Si. Such a huge volume change and crack cause significant capacity loss. Meanwhile, with the crack of Si particles, the conductivity between the electrode and the current collector drops. Moreover, the solid electrolyte interphase (SEI), which is generated during the cycling, reduces the discharge capacity. These issues must be addressed for widespread application of this material. In this work, caramel popcorn shaped porous silicon particles with carbon coating are fabricated by a set of simple chemical methods as active anode material. Si particles are etched to form a porous structure. The pores in Si provide space for the volume expansion and liquid electrolyte diffusion. A layer of amorphous carbon is formed inside the pores, which gives an excellent isolation between the Si particle and electrolyte, so that the formation of the SEI layer is stabilized. Meanwhile, this novel structure enhances the mechanical properties of the Si particles, and the crack phenomenon caused by the volume change is significantly restrained. Therefore, an excellent cycle life under a high rate for the novel Si electrode is achieved.

KEYWORDS: porous Si, carbon coating, Li-ion batteries
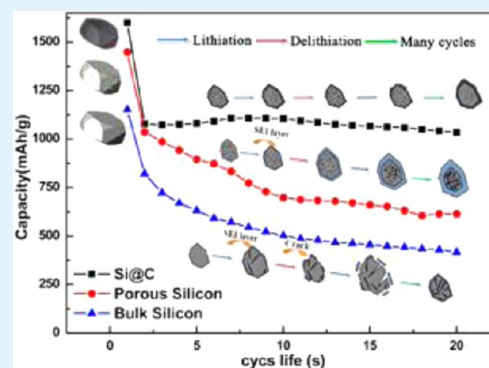
INTRODUCTION

It is universally acknowledged that the lithium ion (Li-ion) battery shows a great promise as a power source and can lead to the energy revolution. Li-ion battery technology has become increasingly important in recent years.[1] Li is one of the most electropositive elements (−3.04 V versus standard hydrogen electrode) and the highest electrochemically active metal. As a result, Li-ion batteries have a higher energy density than other types of rechargeable batteries.[2] Despite their increasing use at the present time, there are still continued commercial interest in and need for developing and improving new electrode materials for Li-ion batteries that would lead to dramatically higher capacity and a longer cycle life, which will allow a wide adoption of hybrid and electric vehicles.[3] However, the traditional carbon-based anode material, such as graphite,[4,5] graphene,[6] and carbon nanotubes,[7] cannot meet the demand for high capacity and energy.

As a result, a long-life, environmentally friendly, low-cost, and reliable anode material for Li-ion batteries is required. As an effort to improve the anode material for Li-ion batteries, silicon (Si) is an ideal candidate with a very high specific capacity and low discharge potential (∼0.5 V vs Li/Li+).[8] Si can alloy with Li and form $Li_{4.4}Si$, which can reach a theoretical capacity as high as 4200 mAh/g,[9] and this is more than 10 times higher than that of commercial graphite anodes. However, the short cycle life of the Si electrode prevents them from being widely used.

Two main reasons have been widely accepted to explain the short cycle life. First, when the Li ions diffuse to the Si anode, the volume of Si will expand to almost 300%−400% of its initial size.[1,10−12] The morphology of Si plays an important role in determining the capacity and cyclability.[13] Such a huge volume change causes significant capacity loss. Moreover, lithium ion intercalation/deintercalation causes great stress in the Si lattice and thus leads to cracking and crumbling of the Si particles. Second, the cycle performance of the Si electrode can also be influenced by the interfacial properties that originate from the formation of a solid electrolyte interphase (SEI) layer,[8,14] which would have a negative effect on the specific capacity. The SEI layer becomes thicker and thicker during cycling, leading to a decreased capacity. As a result, both the low Coulombic efficiency and a decrease in capacity during cycling take place.

To overcome the short cycle life, many efforts have been made. One of the most popular methods is to make a nanostructured Si with a high surface area,[1,2,6−8,10−13,15−17] which could lead to a shorter path length for Li-ion transport and more space for volume change by forming the buffer area during the lithiation and delithiation processes. As a result, a lower overpotential and better reaction kinetics at the electrode

surface are reached.[9] Furthermore, the nanoscale compliant layers increase the stress resilience of Si films; therefore, nanoengineered Si anodes show the potential to enable a new generation of lithium ion batteries with significantly higher reversible capacity.[2] However, nanoscale Si anode material still suffers from a short cycle life because the SEI layer would be generated due to the large surface area contacting with the electrolyte. To improve such a situation, a carbon coating, which can also enhance structural stability,[4,5,7,13,18] is needed. To fabricate a nano Si-carbon, core−shell anode material, the chemical vapor deposition (CVD) method,[16] atomic layer deposition (ALD),[19] or other complex reactions, such as a solvothermal treatment on a bubble template method, are normally used.[20] These methods are expensive and difficult to scale up. For instance, for the CVD method, a little change of the experimental condition, such as the amount of gas flow, would impact the morphology of the product and electrochemical performance significantly.

In this work, caramel popcorn shaped microsize Si particles, with uniform nanosize pores, coated with an amorphous carbon layer are achieved by a set of simple chemical methods. The pores are fabricated by active Au particle catalyzing and HF etching. The carbon layer is similar to the caramel shell, which is achieved by carbonizing the sucrose and adhering both on the surface and inside the pores of the Si particles. The fabrication process is quite easy to control, and most chemicals used are environmentally friendly. To the best of our knowledge, the novel structure of carbon coating both on the particles and inside the pores has never been reported. The carbon-coated porous region can serve as an excellent buffer area for the volume change and stabilize the SEI layer. As a result, high specific capacity and long cycle life have been achieved, which are quite impressive compared with the previous work.[9,10,13,18,21−25,31]

■ EXPERIMENTAL SECTION

Material Synthesis. The overall fabrication process is schematically described in Figure 1. The porous Si powder is fabricated by a
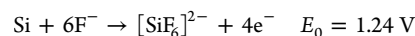

Figure 1. Schematic depiction of the fabrication process for caramel popcorn shaped Si−C particles.
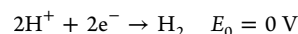
wet chemical method. An amount of 0.6 g of microcrystalline Si (Alfa Aesar) with 1−5 μm crystal size was put into 20 mL of 15 mM sodium tetrachloroaurate dehydrate (NaAuCl$_4$ Premion, 99.99%, metals basis) solution, and then 20 mL of 48% hydrofluoric acid (Alfa Aesar, 99.99%, metals basis) was added. After one hour, Au ions in the AuNaCl$_4$ solution were reduced to nanosize active Au particles, which adhered to the surface of Si to reduce the surface energy, forming the Si−Au precursor. After a vacuum filtration by both distilled water and alcohol, the Si−Au precursor was dried at 70 °C for 12 h. During the reduction of Au ions, Au nanoparticles agglomerated to reduce the surface energy and bulk Au formed because of a better lattice matching

degree. Unlike the very small, well-dispersed Au nanoparticles, the bulk gold is generally regarded to be catalytically inactive.[26] Therefore, the Si−Au precursor was annealed in a tube furnace at 350 °C for 2 h under a flow of Ar to prevent the agglomeration of Au nanoparticles. Then the sample was etched with 20 mL of 40% hydrofluoric acid for 24 h at 70 °C. During the etching process, the gold (Au) deposition plays an important role in the etching process of Si particles. A galvanic displacement reaction takes place because of the Au particles. Subsequently, the Au-deposited Si particles were chemically etched in the 48% HF, at 70 °C for 24 h to make the porous Si structure. In the chemical and galvanic process, Au nanoparticles serve as a cathode, and the Si particles act as an anode. HF exists like the electrolyte, just like a simple electrochemical cell. The reaction of this cell can be described as follows:
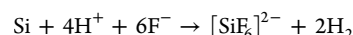
- Anode (Si)

$$Si + 6F^- \rightarrow [SiF_6]^{2-} + 4e^- \quad E_0 = 1.24 \text{ V}$$

- Cathode (Au)

$$2H^+ + 2e^- \rightarrow H_2 \quad E_0 = 0 \text{ V}$$

- The total reaction

$$Si + 4H^+ + 6F^- \rightarrow [SiF_6]^{2-} + 2H_2$$

For the total galvanic reaction, the standard potential is 1.24 V, and the etching process is thermodynamically favorable. As the anode, the Si is continuously dissolved by producing electrons to the surface and reducing the H$^+$ to the H$_2$. Meanwhile, the hydrogen is generated around the Au particles. For this reason, the Si was continuously etched and formed the porous structure.

After etching, the sample was filtrated by distilled water and alcohol and dried for 12 h at 70 °C to obtain the porous Si. Amounts of 0.178 g of as-prepared porous Si, 0.2 g of sucrose, 2 mL of 4 mol/L hydrochloric acid, 4 mL of distilled water, and 8 mL of ethanol were mixed under stirring and ultrasonication for 30 min. The mixture was then stirred for 3 h at 60 °C and dried at 120 °C. At last, the dried mixture with a structure of as-prepared porous Si filled with sucrose was carbonized at 800 °C for 2 h under Ar to obtain the caramel popcorn shaped Si−C particles.

Sample Characterization. Scanning electron microscopy (SEM) with energy dispersive spectroscopy (EDS) was used to characterize morphology and analyze elements of the material (JEOL JSM-7000F). The thickness of the carbon shell and structure of the porous Si were analyzed by a transmission electron microscope (TEM) (Tecnai T12).

Electrochemical Measurements. Each composite anode, including active material, super C65, graphite, and polymer binder (2.5 wt % polyvinylidene fluoride) with a weight ratio of 2:1:6:1, was pasted on the Cu foil directly. The electrochemical testing was against Li foil in a Swagelok cell with stainless steel current collectors. A completed cell consisted of a piece of Li foil, which was pressed onto a collector, two pieces of Celgard 2500 microporous separator placed over the Li foil, and a piece of the composite anode centered over the separator. The cell was sealed with pressure to ensure good contact between the anode and current collector. LiPF$_6$ (1 M) electrolyte solution in ethylene carbonate (EC), diethyl carbonate (DEC), and dimethyl carbonate (DMC) (1:1:1) was used to fabricate cells. Cells were tested with a galvanostat/potentiostat/impedance analyzer (Biologic VMP3). CC (constant current) charging was used, with constant currents C/10, C/5, C/2, C, and 2C applied until cell voltage reached 1.5 V. Each cell was discharged to 0 V at different rates.

■ RESULTS AND DISCUSSION

Sample Morphology. Figure 2 shows the SEM images of the as-received Si, Si−Au precursor, porous Si, and caramel popcorn shaped particles. Figure 2a is the morphology of the original polycrystalline Si particles, which have a particle size in the range of 1−5 μm. Since Si particles are easy to be oxidized, there is SiO$_2$ on Si. SiO$_2$ is easy to remove by hydrofluoric acid in the later step, hence it is expected that it would not affect the
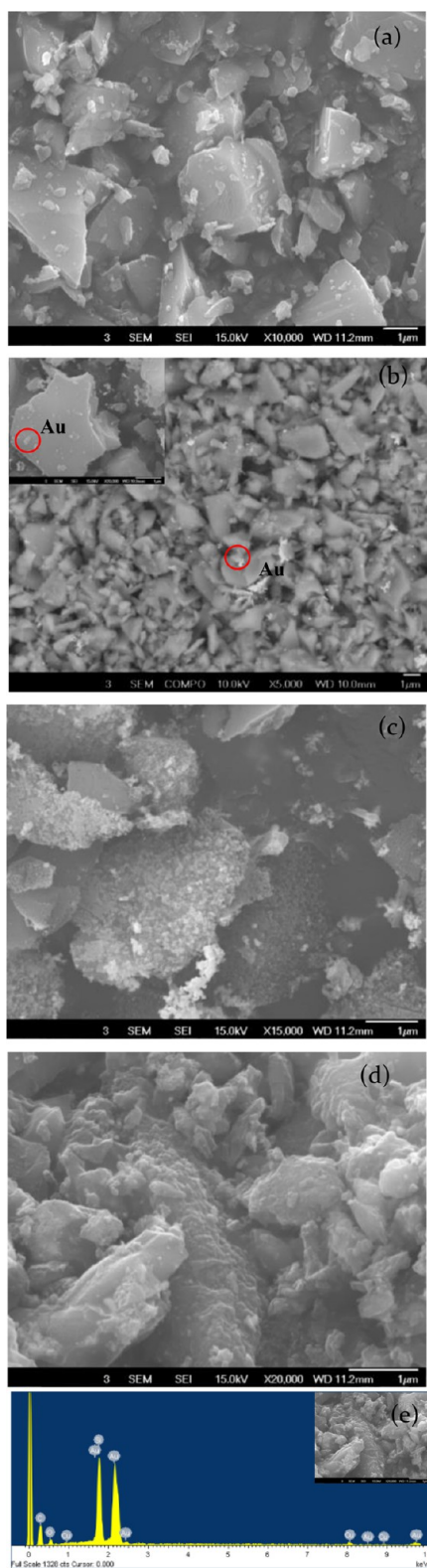
Figure 2. SEM images of Si particles: (a) the as-received Si particle, (b) back-scattered image of the Si−Au precursor with inset secondary electron image, (c) the porous Si particle, (d) the porous Si-carbon, core−shell particle, and (e) the EDS result of the carbon-coated porous Si sample.

performance of our sample. Figure 2b shows the back-scattered image of the Si−Au particle precursor sample. There is an obvious atomic number contrast between Si and well-dispersed

nanosize Au particles. It clearly proves that Au nanoparticles were coated on Si particles. The inset figure is a secondary electron image with a larger magnification. Figure 2c shows the porous Si particle etched for 24 h. It indicates that the nanopores are distributed on the Si surface uniformly, and the diameter of the nanopores is around 50 nm. Those pores can increase the surface area and provide the buffer area when the Si particles suffer from the volume change. Figure 2d exhibits the morphology of caramel popcorn shaped particles, and the surface of particles is coated with carbon. Carbon can strengthen the particle. The thickness of the carbon shell can be well controlled by a fixed amount of sucrose, hydrochloric acid, and the annealing time. Figure 2e shows the EDS spectrum of caramel popcorn shaped active material. The carbon peak is from the carbon shell of the sample, and the Cu peak is from the Cu tape, which holds the sample.

Figure 3a and Figure 3b are the TEM images with different magnifications for the porous Si. They show that nanopores exist on both the Si surface and inside, which has never been reported. The diameter of the nanopores is around 50 nm which is consistent with the SEM results. The dark spots on the sample are Au active particles. The images indicate that most of the Au active nanoparticles are around 10 nm in diameter, and the uniformity of the Au particle size is partially due to the annealing process.[17,26] It is reported that the uniform Au particles have a great effect on the morphology of the porous Si.[27] These nanopores can accommodate the large volume changes and maintain the mechanical integrity of the Si particles during cycling. Si utilization can also be improved significantly when comparing with the common micrometer size Si particles due to a great improvement of the contact area between Si and electrolyte.

Figure 3c and Figure 3d are the TEM images of the caramel popcorn shaped Si particles with different magnifications. An obvious boundary (shown in Figure 3c) between the Si particles and amorphous carbon is observed due to the difference in their structure (Si is crystalline and carbon is amorphous) and the atomic number contrast. It shows that carbon is coated not only on the surface of the porous Si particle but also inside the pores. On the other hand, the mechanical behavior of the sample would become better, and the SEI layer is stabilized by carbon layer isolation.

Electrochemical Test. Figure 4a compares the charge−discharge curves at the voltage range of 0−1.5 V under the current density of 0.2 C for micro Si, porous Si, and caramel popcorn shaped samples. All three samples are pasted on the Cu foil directly. The discharge capacity of Si, porous Si, and caramel popcorn shaped particles in the first cycle is 1152, 1448, and 1600 mAh/g, respectively, and drops to 821, 1036, and 1078 mAh/g, respectively, in the second cycle. The large drop in the first cycle is due to the formation of the SEI layer. The discharge capacity for both the carbon-coated Si and the porous Si is significantly higher than the original Si powder. Such a result can be ascribed to the higher ion exchange efficiency with the higher surface area.[28] High Coulombic efficiency in the first cycle is observed from all the samples including bulk Si (98.5%), porous Si (99.4%), and Si-carbon particle (95.2%). In the second cycle, the efficiency is 98.7%, 98.3%, and 94.5%, respectively. The results suggest that an almost complete delithiation is followed after lithiation in the first two cycles for all the samples.[23,29]

After 20 cycles, the Coulombic efficiency of the three samples is 96.8%, 97.1%, and 96.4% for bulk Si, porous Si, and
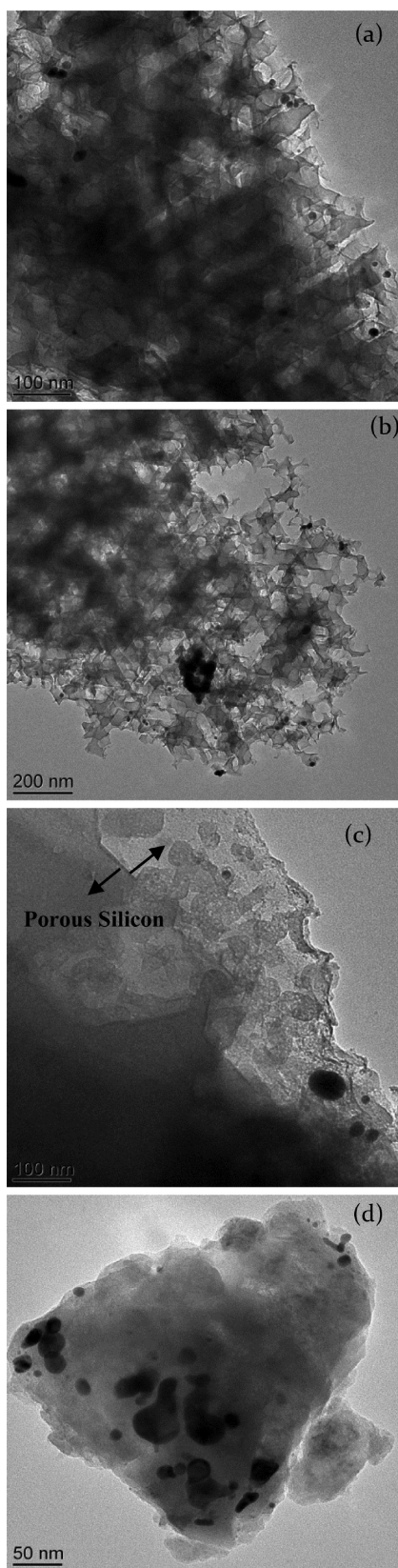
Figure 3. TEM images of the Si particle. (a), (b) Porous Si particle at different magnification. (c), (d) Porous Si-carbon, core—shell material at different magnification.

Si-carbon particle, respectively. The specific discharge capacity is 416, 613, and 1034 mAh/g, respectively, and the capacity
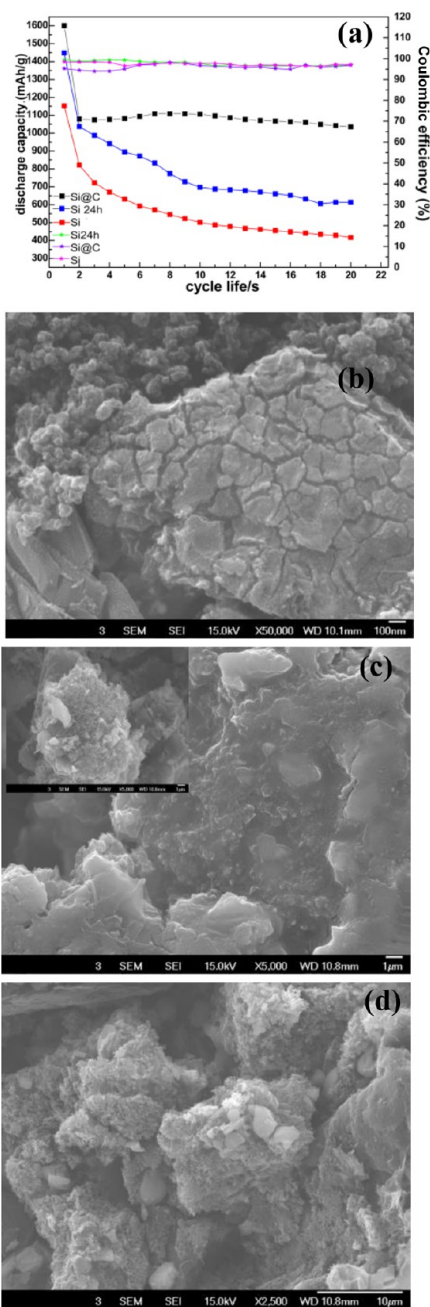

Figure 4. (a) Comparison of galvanostatic charge—discharge of original Si, porous Si, and Si-carbon shaped particle. (b) SEM image of original Si, (c) porous Si, and (d) Si-carbon coating particle after 20 cycles under 0.2 C.

drop in 20 cycles is 49.3%, 40.8%, and 4.0%, which corresponds to 2.5%, 2.0%, and 0.2% drops per cycle, respectively. All of the data indicate that the caramel popcorn shaped material demonstrated a much more stable cycling performance than the other two samples.

The above data indicate that although the difference of the discharge capacity in the first two cycles is not very obvious a sharp drop is observed in the first 20 cycles for the as-received Si particle and porous Si particle. It is seen that porous Si only shows very limited improvement to stabilize the cycle life, and the reason is that the crack of the Si particle as well as the formation of the SEI layer of the simple porous structure lead to the capacity fading. Furthermore, Mai et al. reported that the

crystalline Si lost its order and became a metastable amorphous Li$_x$Si alloy after lithiation.[30] Figure 4b shows the original Si particle after 20 cycles with a current density of 0.2 C, indicating that the crack occurs everywhere because of the volume expansion and contraction, and the particles pulverize. As a result, the Si particles lose the contact with the current collector and each other. Figure 4c shows the porous Si particle after 20 cycles with a current density of 0.2 C. Upon the basis of the image, we can see that the SEI layer adheres to the porous Si particles, which leads to the decreased capacity. The inset image is the porous sample after removing the SEI layer by dilute HCl washing. The inset image indicates that the porous Si still retains the original morphology after 20 cycles. This result supports that the porous structure can provide the buffer area to improve the volume change efficiently, although the significant capacity drop takes place. Figure 4d shows the morphology of the caramel popcorn shaped material after 20 cycles with a current density of 0.2 C. The image demonstrates that the active material retains the original morphology, and neither obvious SEI layer nor cracks are observed. Therefore, caramel-shaped active material can overcome the crack and stabilize the SEI layer efficiently.

For the original Si particles, the main mechanism of its poor electrochemical performance is the crack due to the volume expansion and contraction during cycling. As Figure 5a shows,
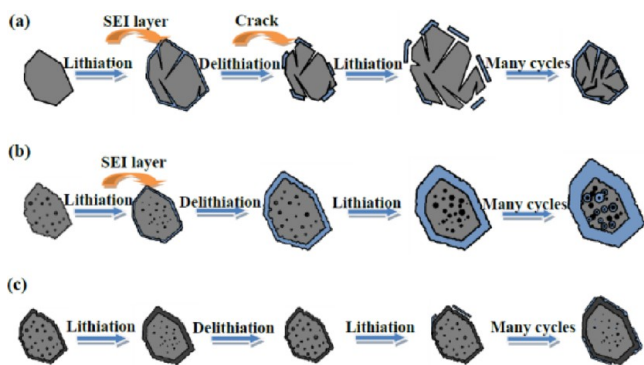

Figure 5. Lithiation−delithation schematic diagram for (a) original Si, (b) porous Si, and (c) caramel popcorn shaped active material.

during the lithiation process, the volume of the Si particle expands. Meanwhile, the SEI layer forms and adheres to the surface of Si. During the delithiation process, the volume of the particle contracts. Since Si is brittle, the crack occurs. At the same time, the SEI layer is broken at the delithiation stage. Therefore, for the first 20 cycles, the cracks occur before the SEI layer becomes too thick. So the cracks mainly lead to the capacity drop, which can also be seen in Figure 4b.

For the porous Si particle, the main mechanism of the capacity drop is the formation of the SEI layer as shown in Figure 5b. Since the surface of Si is covered with an inactive layer consisting of Si oxide (−Si−O−Si−) and silanol (−Si−OH), the surface after cycling is passivated with the SEI layer, which is composed of the decomposition products of liquid electrolyte. With cycling, the SEI layer becomes thicker and thicker. As stated before, the SEI layer can be broken at the delithiated state due to the change of the surface area, which is caused by the volume change. For the original Si particles, the volume of active material changes significantly, and the SEI layer is not obvious. However, for the porous Si particles, there is a great surface area that can be contacted with the electrolyte,
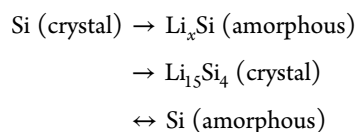
and the nanopores can provide enough buffer area for the volume change. As the result, the thickness of the SEI layer increases significantly during the cycling. Thus, the capacity drop for porous Si is mainly because of the formation of the SEI layer, which can be seen in Figure 4c.

Figure 5c shows the mechanism of caramel popcorn shaped particles to stabilize the electrochemical properties during cycling. A layer of carbon coating could both improve the mechanical behavior of the sample and stabilize the SEI layer. As we mentioned above, the cycle performance could be enhanced by controlling the SEI layer and volume expansion. The carbon coating could improve this phenomenon efficiently by isolating the Si surface from the electrolyte and enhancing the mechanical behavior of the porous Si particles. The pores are also coated with carbon, which can protect the inside surface efficiently. Furthermore, the poor electronic conductivity of the Si could be improved by the carbonization. Therefore, during the process of lithiation and delithiation, the volume remains stable, and carbon stabilizes the SEI layer. The formation of the SEI layer on the surface of the caramel popcorn shaped active material is harder than both bulk and porous Si. In other words, the SEI layer, which is formed after many cycles, is thinner than other samples. Therefore, we expect that the caramel popcorn shaped active material is more stable, and its cycle life is much longer than others.

Figure 6a shows the cycle performance of the caramel popcorn shaped active material under the current density of 0.1 C from 0 to 1.5 V. The average efficiency and discharge capacity from the third cycle to the 100th cycle are 96.77% and 1563 mAh/g, respectively. The inactivity on the initial stage is due to the formation of the SEI layer. With cycling, the SEI layer becomes stable because the interface between the Si particle and electrolyte is isolated by the carbon shell. For this reason, high Coulombic efficiency occurred. The good electrochemical performance is also due to good mechanical support and an efficient electron pathway in the core−shell structure. The much less pulverization during the charge and discharge is caused by a homogeneous insertion of Li ions.

Moreover, we investigate the rate capabilities of the caramel popcorn shaped active material, which was pasted on the Cu foil directly. Figure 6b shows the charge and discharge curves observed at the C/20, C/10, C/5, C/2, 1C, and 2C rates. The inefficiency at the beginning stage can be attributed to the formation of the SEI layer, which becomes stable in the further. The high reversible capacity is partly attributed to the carbon shell with low crystallization, which facilitates fast transmission of Li ions.[33] Meanwhile, the porous structure can give a large enough buffer area.

Figure 6c shows the cyclic voltammetry (CV) test of the caramel-shaped sample for three cycles at 1 mV/s. The mismatch part in the first cycle is due to the polarization and the formation of the SEI layer on the anode side. The two redox peaks are around 0.26 and 0.38 V. It is related to the following conversion reactions.

$$\text{Si (crystal)} \rightarrow \text{Li}_x\text{Si (amorphous)}$$
$$\rightarrow \text{Li}_{15}\text{Si}_4 \text{ (crystal)}$$
$$\leftrightarrow \text{Si (amorphous)}$$

The controlled SEI layer growth can also be supported through electrochemical impedance spectroscopy (EIS). It is well-known that the rapid growth of the SEI layer can result in
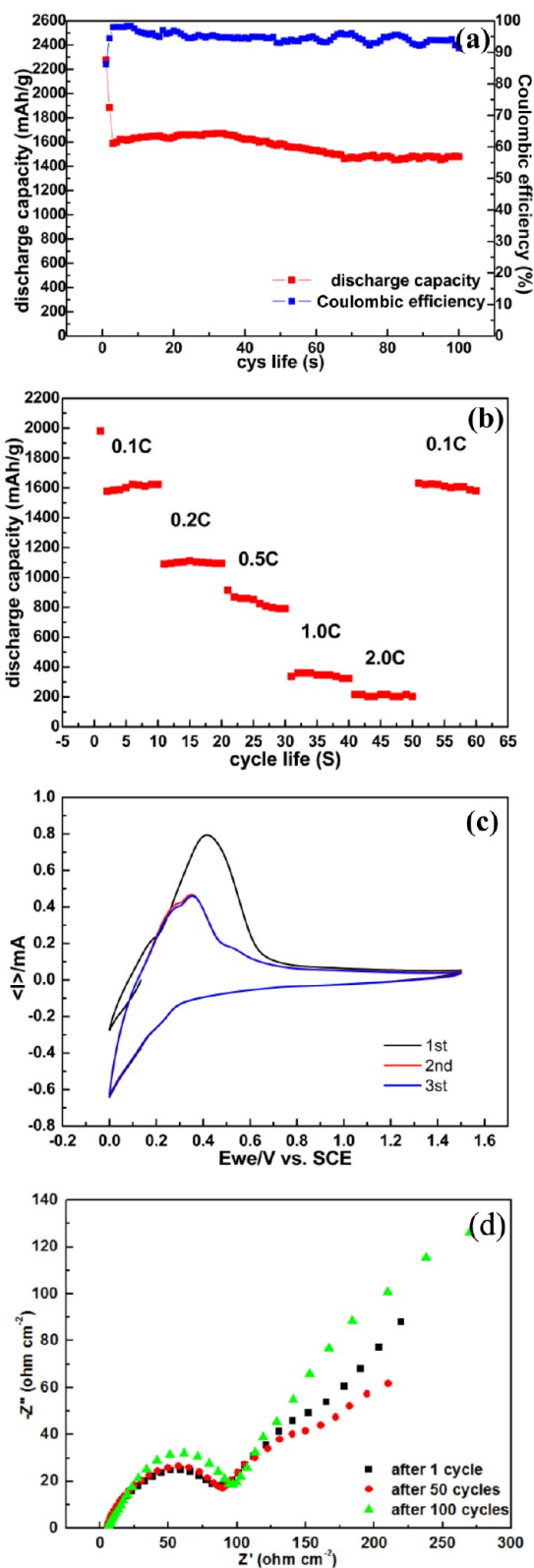
an increase of the impedance as well as a decrease of the capacity. The EIS was employed to determine the impedance of the electrodes, which is shown in Figure 6d. The semicircle located on the high-frequency region reflects the interfacial charge transfer resistance, which is attributed to the SEI layer. The straight line in the low-frequency part represents the lithium diffusion resistance. As shown in Figure 6d, the impedance almost keeps constant after 1, 50, and 100 cycles. It indicates that the popcorn structure can stabilize the SEI layer very well.[32]

■ CONCLUSION

In summary, through a combination of material synthesis, electrochemical testing, and spectroscopic analysis, we developed a caramel popcorn shaped Si-carbon material and a novel anode structure to overcome the capacity fading of the Si electrode. The porous structure can provide enough buffer area to overcome the volume change during cycling; the carbon shell is coated both on the surface of the Si particles and inside the pores, so that the carbon can stabilize the SEI layer efficiently as well as enhance the mechanical properties of the porous Si particles. These results are much better than the received original microsize crystal Si and porous Si particle as well as some other published results.[34−37] Our results also demonstrated that the cracking and SEI layer need to be solved to improve the cycle life and capacity of Si-based anode material. Due to its versatility, the caramel popcorn shaped material may be extended to other high-capacity electrode materials with large volume variation and poor cyclability.

■ AUTHOR INFORMATION

Corresponding Author
*E-mail: yanwang@wpi.edu.

Notes

The authors declare no competing financial interest.

■ ACKNOWLEDGMENTS

■ REFERENCES

(1) Park, M.-H.; Kim, M. G.; Joo, J.; Kim, K.; Kim, J.; Ahn, S.; Cui, Y.; Cho, J. *Nano Lett.* **2009**, *9*, 3844−3847.
(2) Teki, R.; Datta, M. K.; Krishnan, R.; Parker, T. C.; Lu, T.-M.; Kumta, P. N.; Koratkar, N. *Small* **2009**, *5*, 2236−2242.
(3) Peterson, S. B.; Apt, J.; Whitacre, J. F. *J. Power Sources* **2010**, *195*, 2385−2392.
(4) Yoshio, M.; Wang, H.; Fukuda, K.; Hara, Y.; Adachi, Y. *J. Electrochem. Soc.* **2000**, *147*, 1245−1250.
(5) Wang, H.; Yoshio, M. *J. Power Sources* **2001**, *93*, 123−129.
(6) Yoo, E.; Kim, J.; Hosono, E.; Zhou, H.-S.; Kudo, T.; Honma, I. *Nano Lett.* **2008**, *8*, 2277−2282.
(7) Chen, J.; Liu, Y.; Minett, A. I.; Lynam, C.; Wang, J.; Wallace, G. G. *Chem. Mater.* **2007**, *19*, 3595−3597.
(8) Liu, N.; Wu, H.; McDowell, M. T.; Yao, Y.; Wang, C.; Cui, Y. *Nano Lett.* **2012**, *12*, 3315−3321.
(9) Liu, J.; Xue, D. *Nanoscale Res. Lett.* **2010**, *5*, 525−1534.
(10) Wu, H.; Zheng, G.; Liu, N.; Carney, T. J.; Yang, Y.; Cui, Y. *Nano Lett.* **2012**, *12*, 904−909.
(11) Ge, M.; Rong, J.; Fang, X.; Zhou, C. *Nano Lett.* **2012**, *12*, 2318−2323.
(12) Cui, L.-F.; Ruffo, R.; Chan, C. K.; Peng, H.; Cui, Y. *Nano Lett.* **2008**, *9*, 491−495.

Figure 6. (a) Cycle performance of the caramel popcorn shaped active material. (b) Rate capabilities of the caramel popcorn shaped material. (c) The cyclic voltammetry (CV) test of the caramel shaped sample for three cycles at 1 mV/s. The mismatch part in the first cycle is due to the polarization and the formation of the SEI layer on the Si electrode side. (d) The impedance test of the caramel popcorn shaped material.

(13) Xiao, J.; Xu, W.; Wang, D.; Choi, D.; Wang, W.; Li, X.; Graff, G. L.; Liu, J.; Zhang, J.-G. *J. Electrochem. Soc.* **2010**, *157*, A1047−A1051.

(14) Lee, Y. M.; Lee, J. Y.; Shim, H.-T.; Lee, J. K.; Park, J.-K. *J. Electrochem. Soc.* **2007**, *154*, A515−A519.

(15) Zheng, Y.; Yang, J.; Wang, J.; NuLi, Y. *Electrochim. Acta* **2007**, *52*, 5863−5867.

(16) Ng, S. H.; Wang, J.; Wexler, D.; Konstantinov, K.; Guo, Z. P.; Liu, H. K. *Angew. Chem., Int. Ed.* **2006**, *45*, 6896−6899.

(17) Ng, S. H.; Wang, J.; Wexler, D.; Chew, S. Y.; Liu, H. K. *J. Phys. Chem. C* **2007**, *111*, 11131−11138.

(18) Zuo, P.; Yin, G.; Ma, Y. *Electrochim. Acta* **2007**, *52*, 4878−4883.

(19) Baggetto, L.; Oudenhoven, J. F. M.; van Dongen, T.; Klootwijk, J. H.; Mulder, M.; Niessen, R. A. H.; de Croon, M. H. J. M.; Notten, P. H. L. *J. Power Sources* **2009**, *189*, 402−410.

(20) Ma, H.; Cheng, F.; Chen, J. Y.; Zhao, J. Z.; Li, C. S.; Tao, Z. L.; Liang, J. *Adv. Mater.* **2007**, *19*, 4067−4070.

(21) Gao, P.; Fu, J.; Yang, J.; Lv, R.; Wang, J.; Nuli, Y.; Tang, X. *Phys. Chem. Chem. Phys.* **2009**, *11*, 11101−11105.

(22) Yin, Y.-X.; Xin, S.; Wan, L.-J.; Li, C.-J.; Guo, Y.-G. *J. Phys. Chem. C* **2011**, *115*, 14148−14154.

(23) Dimov, N.; Kugino, S.; Yoshio, M. *Electrochim. Acta* **2003**, *48*, 1579−1587.

(24) Feng, X.; Yang, J.; Gao, P.; Wang, J.; Nuli, Y. *RSC Adv.* **2012**, *2*, 5701−5706.

(25) Hwang, T. H.; Lee, Y. M.; Kong, B.-S.; Seo, J.-S.; Choi, J. W. *Nano Lett.* **2012**, *12*, 802−807.

(26) Haruta, M. *Chem. Rec.* **2003**, *3*, 75−87.

(27) Megouda, N.; Hadjersi, T.; Piret, G.; Boukherroub, R.; Elkechai, O. *Appl. Surf. Sci.* **2009**, *255*, 6210−6216.

(28) Kirkland, J. J. *J. Chromatogr. Sci.* **1969**, *7*, 361−365.

(29) Obrovac, M. N.; Krause, L. J. *J. Electrochem. Soc.* **2007**, *154*, A103−A108.

(30) Mai, L.; Dong, Y.; Xu, L.; Han, C. *Nano Lett.* **2010**, *10*, 4273−4278.

(31) Yang, J.; Wang, B. F.; Wang, K.; Liu, Y.; Xie, J. Y.; Wen, Z. S. *Electrochem. Solid-State Lett.* **2003**, *6*, A154−A156.

(32) Fan, J.; Fedkiw, P. S. *J. Power Sources* **1998**, *72*, 165−173.

(33) Howlett, P. C.; MacFarlane, D. R.; Hollenkamp, A. F. *Electrochem. Solid State Lett.* **2004**, *7*, A97−A101.

(34) Shen, L.; Guo, X.; Fang, X.; Wang, Z.; Chen, L. *J. Power Sources* **2012**, *213*, 229−232.

(35) Ge, M.; Rong, J.; Fang, X.; Zhang, A.; Lu, Y.; Zhou, C. *Nano Res.* **2013**, *6*, 174−181.

(36) Thakur, M.; Isaacson, M.; Sinsabaugh, S. L.; Wong, M. S.; Biswal, S. L. *J. Power Sources* **2012**, *205*, 426−432.

(37) Bang, B. M.; Lee, J.-I.; Kim, H.; Cho, J.; Park, S. *Adv. Energy Mater.* **2012**, *2*, 878−883.